Pure Appl. Geophys. 175 (2018), 1951–1969

https://doi.org/10.1007/s00024-018-1878-x

Pure and Applied Geophysics

Tides in the Black Sea: Observations and Numerical Modelling

Igor P. Medvedev[1,2]

Abstract—Longterm hourly data from 28 tide gauges were used to examine the main features of tides in the Black Sea. The tides in this basin are directly caused by tide-generating forces and the semidiurnal tides prevail over diurnal tides. Based on the Princeton Ocean Model (POM), a numerical model of tides in the Black Sea and adjacent Sea of Azov was developed and found to be in good agreement with tide gauge observations. Detailed tidal charts for amplitudes and phase lags of the major tidal harmonics in these two seas were constructed. The results of the numerical modelling and observations reveal for the semidiurnal tides the presence of an amphidromy with clockwise rotation and another one with counterclockwise rotation for the diurnal tides, both located in the central part of the sea near the Crimean Peninsula. Therefore, for this part of the sea the amplitudes of harmonics M_2 and K_1 are less than 0.1 cm. Relatively larger M_2 amplitudes are observed on the east and west coasts of the sea (2–3 cm). The maximum amplitude of the harmonic M_2 was found at Karkinit Bay—up to 4.5 cm—while the maximum tidal range varies from 1 cm near the Crimean Peninsula to 18–19 cm in the Dnieper–Bug Estuary and Karkinit Bay. Radiational tides, initiated mainly by sea breezes, make an important contribution to the formation of tidal oscillations in the Dnieper–Bug Estuary.

Key words: Tides, tide gauges, Black Sea, Sea of Azov, amphidromic points, sea level spectra, numerical modelling, radiational tides, seiches.

1. Introduction

Tides are one of the most important types of ocean water motions. Tidal oscillations are formed under the influence of the tide-generating forces of the Moon and the Sun. The variability of these forces over time leads to the periodic oscillations of the sea level and currents. Tides in the World Ocean can be represented as the sum of two types of motions: (1) the *co-oscillating* tide caused by the tidal oscillations incoming from an adjacent basin, and (2) the *independent* tide representing the direct response of the water body of the basin to the tide-generating forces (Defant 1961). Marginal seas are typically dominated by co-oscillating tides generated by tidal waves penetrating from the ocean. In the mostly enclosed seas, tidal waves from adjacent basins have negligible influence, and independent tides strongly prevail (Defant 1961; Medvedev et al. 2016).

The Black Sea is one of the most isolated seas of the World Ocean. It is connected with the Mediterranean Sea through the Bosphorus, the Sea of Marmara, and the Dardanelles. It is also linked with the Sea of Azov through Kerch Strait. Narrow straits do not enable the penetration of sea level variations (including tides) from the Mediterranean Sea into the Black Sea. Tides in the Black Sea are caused directly by tidal forces and are of the second type: *independent*. The amplitudes of major tidal harmonics are known to be only a few centimetres (Defant 1961; Fomicheva et al. 1991; Medvedev et al. 2016). But, despite this fact, their accurate assessment is crucial for understanding the general dynamics of the Black Sea including many processes that depend upon the tide. Barotropic tides are responsible for formation of internal waves that can be significant, especially in the upper layer and, therefore, strongly influence various hydrobiological processes and bioproductivity of the sea.

The study of tidal oscillations in the Black Sea started in the first part of the twentieth century (Sterneck 1912, 1922, 1926; Orlov 1923; Kurchatov 1925; Proudman 1928; Endrös 1932). Based on the data obtained in previous studies, Albert Defant (1961) constructed a co-tidal chart of the semidiurnal tide in the Black Sea. According to his study, it has the character of an amphidromic system with

[1] P.P. Shirshov Institute of Oceanology, 36 Nakhimovsky Pr., 117997 Moscow, Russia. E-mail: patamates@gmail.com
[2] Fedorov Institute of Applied Geophysics, 9 Rostokinskaya Street, 129128 Moscow, Russia.

clockwise rotation. Engel (1974) numerically modelled the M_2 co-tidal chart for the Black Sea. Further studies (Fomicheva et al. 1991; Alpar and Yüce 1998) based on analysis of observation series confirmed the high accuracy of these co-tidal charts. Subsequently, both diurnal and semidiurnal tidal constituents were reliably identified in the sea level spectra for the Black Sea (German 1970; Mungov 1981; Maramzin 1985; Ivanov and Yastreb 1989; Fomicheva et al. 1991). Yüce (1993) estimated the amplitudes of the diurnal, semidiurnal, and long-period (fortnightly M_f and monthly M_m) tides in the Sea of Marmara and in the Bosphorus. Yüce (1996) distinguished a well-defined peak at diurnal tidal frequency in current speed spectrum in the Bosphorus. Book et al. (2010), using ADCP current measurements, showed that current fluctuations at tidal frequencies also play a role in the Turkish Strait System, reaching 20% of the total variance of the current in the mid-water column of the southern Dardanelles Strait.

It was shown by Mungov (1981), Krsteva (1981), and Fomicheva et al. (1991) that sea-breeze effects play a significant role in the formation of diurnal sea level oscillations in the Black Sea. However, the relative role of tidal and breeze forces in the formation of diurnal tide has not yet been fully studied. Thus, the formation mechanism of diurnal tides in the Black Sea is still poorly understood. Recently, Medvedev and Kulikov (2016) studied the spectrum of sea level oscillations of the Black Sea based on longterm hourly series of observations at 23 tide gauges and found marked tidal spectral peaks for diurnal and semidiurnal clusters of harmonics. These tide gauge series, complemented by data from Turkey served as the basis for the present study of tidal sea level oscillations in the Black Sea.

2. Data

For the analysis of tidal oscillations, hourly observations for 28 coastal tide gauges have been used (Table 1). The tide gauges are located along the coasts of Russia, Ukraine, Georgia, and Turkey (Fig. 1). Data from post-Soviet Union era tide gauges were mainly obtained from the Russian portal "The Unified State System of Information on the World Ocean" (in Russian ESIMO, http://www.esimo.ru). The tide gauge records along the Turkish coast were collected by the Turkish National Sea Level Monitoring System (TUDES, http://tudes.hgk.msb.gov.tr/tudesportal). For some tide gauges, the archive of hourly sea level records covers the 1970s and 1980s decades of the twentieth century. Certain sites where tide gauges were located have changed their names in recent decades; therefore, in Table 1, both the old and new names of tide gauges are presented. The duration of the observational sea level series varies from 3 to 38 years (Table 1). Data for all stations have been adjusted to the Coordinated Universal Time (UTC). The series were thoroughly checked, all spikes and shifts were eliminated; short gaps (shorter than a day) were filled with predicted tidal sea level oscillations. We excluded from our analysis the yearly series with long gaps or low-quality data. The time coverage of the data which were used in the harmonic analysis of tides is presented in the last column of Table 1. Red circles in Fig. 1 indicate the Bulgarian tide gauges Burgas and Varna. The harmonic constants for these sites were taken from Ivanov (2015).

3. The Spectral Analysis of the Sea Level Oscillations

The spectral properties of sea level variability in the Black Sea were described in detail by Medvedev and Kulikov (2016). The authors showed that seiches (eigen oscillations) and tides in the Black Sea have significantly different spectral properties. Tides appear in the spectrum as sharp, discrete peaks with frequencies of major tidal harmonics, while seiches have a character of relatively broader increase at the continuous part of the spectrum (continuum) at resonant (eigen) frequencies. Special attention was given to a spectral peak located between the diurnal and semidiurnal frequencies. The period of this peak coincides with the inertial period. At higher frequencies in the sea level spectrum in the Black Sea, wide maxima associated with eigen modes of the sea prevail.

The main focus of the present study is a detailed analysis of sea level spectra at tidal frequencies. Our

Table 1

Tide gauges used in this study for the analysis of tidal sea level oscillations in the Black Sea

No.	Tide gauge	City	Latitude (°N)	Longitude (°E)	Time coverage (years)	Harmonic analysis (years)
1	Bolshoe	Bolshoe	45.2	29.7	1977–1984	1977–1982
2	Vilkovo	Vylkove	45.4	29.6	1977–1984	1977–1981, 1983
3	Prorva	Prorvin	45.5	29.7	1977–1984	1977–1983
4	Belgorod-Dnestrovskiy	Bilhorod-Dnistrovskiy	46.2	30.4	1977–1995	1977–1992, 1994
5	Paromnaja Pereprava	Paromnaja Pereprava	46.3	30.6	1980–1995	1980–1995
6	Illichivsk	Chornomorsk	46.3	30.7	1977–1995	1977–1995
7	Odessa	Odesa	46.5	30.8	1977–1995	1977–1992, 1994–1995
8	Ochakov	Ochakiv	46.6	31.6	1977–1995	1978–1995
9	Heroyskoe	Heroiske	46.5	31.9	1985–1995	1985–1987, 1989–1995
10	Nikolaev	Mykolaiv	47.0	32.0	1977–1995	1977–1995
11	Stanislav	Stanislav	46.6	32.2	1989–1991	1990
12	Kasperovka	Kasperovka	46.6	32.3	1977–1995	1977–1995
13	Kherson	Kherson	46.6	32.6	1977–1995	1977–1995
14	Sevastopol	Sevastopol	44.6	33.5	1977–1995	1977–1991, 1993–1995
15	Yalta	Yalta	44.5	34.2	1977–1995	1977–1995
16	Feodosia	Feodosia	45.0	35.4	1977–1995	1977–1995
17	Gelendzhik	Gelendzhik	44.6	38.1	1977–1992	1977–1987, 1991
18	Tuapse	Tuapse	44.1	39.1	1977–2014	1977–1987, 1989, 1991–1996, 2007–2012
19	Sochi	Sochi	43.5	39.8	1977–1995	1977–1987, 1989, 1991–1995
20	Kulevi	Kulevi	42.3	41.7	1977–1979	1978
21	Poti (Rioni)	Poti (Rioni)	42.2	41.7	1977–1979	1978
22	Poti	Poti	42.1	41.6	1977–1991	1977–1990
23	Batumi	Batumi	41.7	41.6	1977–1991	1977–1990
24	Trabzon	Trabzon	41.0	39.7	2002–2017	2003–2004, 2006–2008 2010–2015, 2017
25	Sinop	Sinop	42.0	35.2	2005–2017	2006
26	Amasra	Amasra	41.7	32.4	2001–2017	2013–2017
27	Şile	Şile	41.2	29.6	2008–2017	2009–2016
28	Iğneada	Iğneada	41.9	28.0	2002–2017	2012–2014
29	Burgas	Burgas	42.5	27.5	2013–2014	2013–2014
30	Varna	Varna	43.2	27.9	2013–2014	2013–2014

spectral procedure is similar to that described by Thomson and Emery (2014) (see Medvedev and Kulikov 2016; Medvedev et al. 2017 for details), and is based on the Fast Fourier Transform of long sea level observational series. To improve the spectral estimates we used the spectral Kaiser–Bessel (KB) window with half-window overlaps prior to the Fourier transform. The length of the window was $N = 8192$ h (spectral resolution $\Delta f \approx 0.00293$ cpd). For Sochi, the window length was smaller: $N = 4096$ h ($\Delta f \approx 0.00586$ cpd). The confidence intervals in the spectra depended on the number of degrees of freedom (v) which varied depending on the total length of the series: $v = 58$ for Batumi, $v = 62$ for Trabzon, $v = 78$ for Illichivsk, Kasperovka, and Feodosia, and $v = 92$ for Sochi.

Fig. 2 presents the spectra of sea level oscillations for six tide gauges which are located in various parts of the sea: Illichivsk, Sochi, Kasperovka, Batumi, Feodosia, and Trabzon. Tides are identified in the sea level spectra as narrow and sharp peaks at diurnal and semidiurnal frequencies. In the semidiurnal frequency band the principal lunar semidiurnal constituent M_2 (12.42 h), the principal solar semidiurnal constituent S_2 (12.00 h), and the larger elliptical lunar constituent N_2 (12.65 h) dominate. A tidal peak

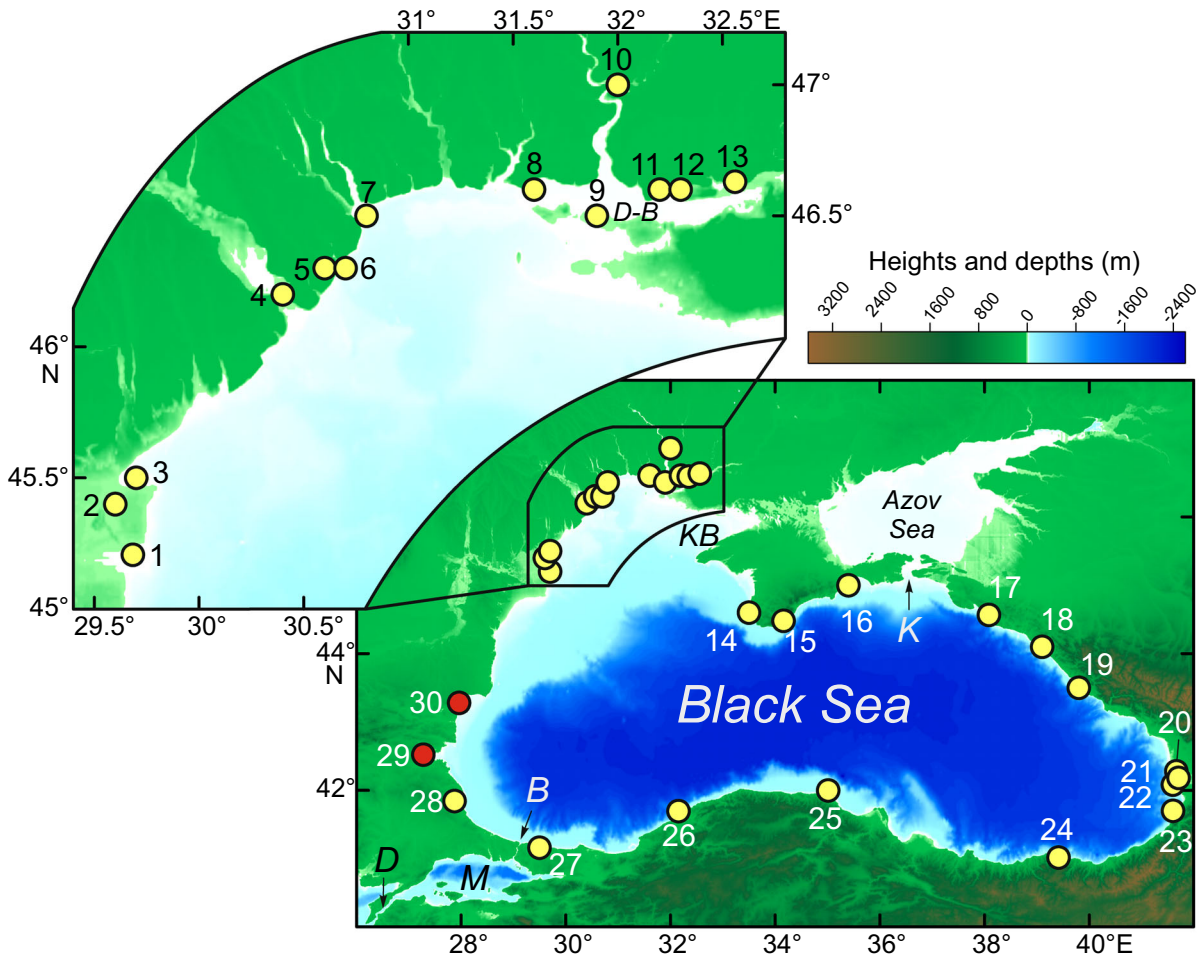

Figure 1
The locations of the tide gauge stations that have been used in this study. Numbers (1–30) in the figure correspond to stations in Table 1. Red dots (29–30) are the Bulgarian tide gauges (Ivanov 2015). Other designations: *M* the Sea of Marmara, *B* the Bosphorus, *D* the Dardanelles, *K* the Kerch Strait, *KB* Kirkinit Bay, and *D–B* the Dnieper–Bug Estuary

with a frequency of $\sim$ 1 cpd prevails in the diurnal tidal band in all considered spectra; it may be related either to the gravitational lunisolar diurnal constituent K_1 (23.93 h) or to the radiational diurnal constituent S_1 (24.00 h). Also, the peak corresponding to the principal lunar diurnal constituent O_1 (25.82 h) is evident in all the spectra (Fig. 2).

On the east coast of the Black Sea, the semidiurnal tides are predominant (Fig. 2b, d, f). According to Defant (1961), Engel (1974) and Fomicheva et al. (1991), the nodal point of the semidiurnal tidal amphidromic system is located in the central part of the Black Sea, so the semidiurnal tides near the coast of the Crimea and in the central part of the Turkish coast are weak. On the sea level spectra at Feodosia, the Crimean Peninsula (Fig. 2e), the energy of harmonic M_2 is lower than the K_1 energy and much smaller than the M_2 energy on the western (Fig. 2a) and eastern coasts of the Black Sea (Fig. 2b, d, f).

The northwestern part of the Black Sea is characterized by the complex structure of the tides. At the Illichivsk spectrum (Fig. 2a), the M_2 and S_2 semidiurnal tidal peaks exceed those of diurnal harmonics K_1 and O_1. In contrast, at Kasperovka, (Fig. 2c), which is located at the head of the Dnieper Estuary, the diurnal peak with a period of $\sim$ 24 h

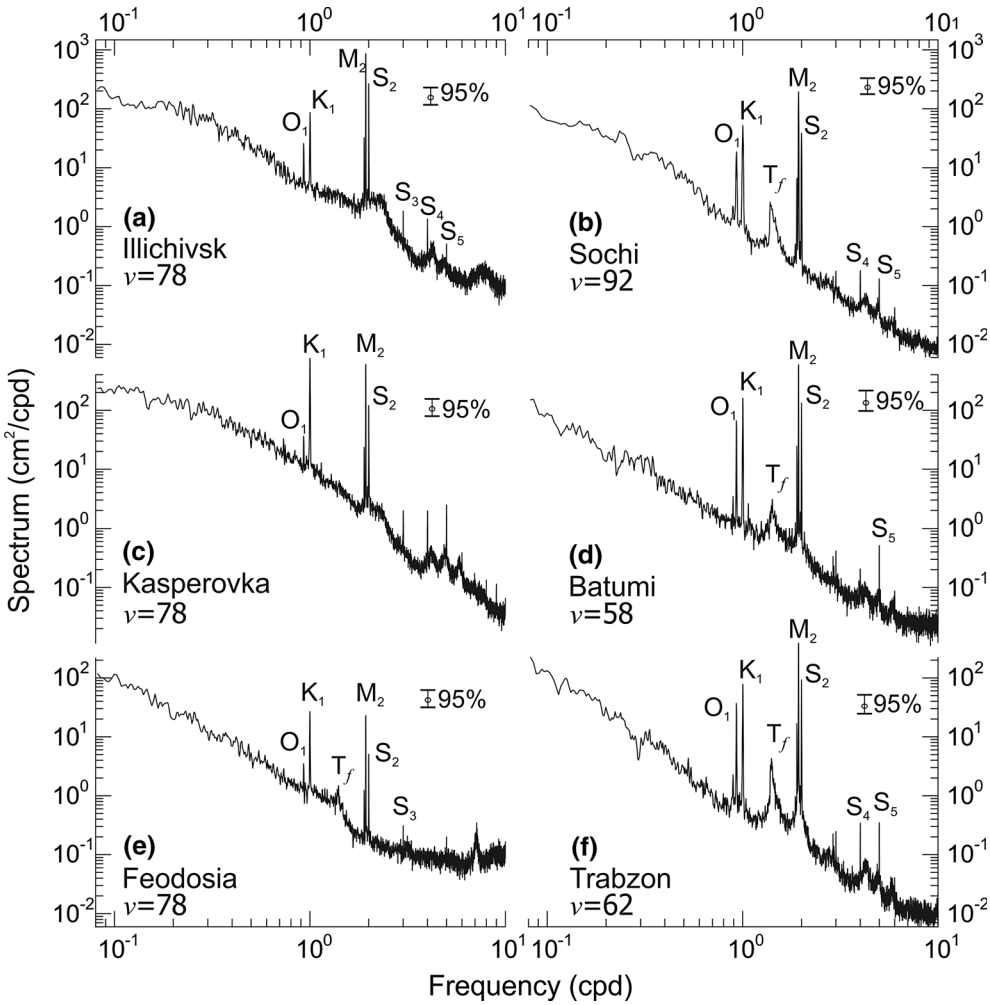

Figure 2
The spectra of the sea level oscillations at stations Illichivsk (**a**), Sochi (**b**), Kasperovka (**c**), Batumi (**d**), Feodosia (**e**), and Trabzon (**f**). Noted peaks correspond to the main tidal harmonics (O_1, K_1, M_2, and S_2), inertial oscillations of sea level (T_f) and radiational harmonics (S_{3-5}). The number of degrees of freedom in the spectral calculations is specified (ν), and the corresponding confidence intervals are shown

substantially exceeds the main semidiurnal peaks. It appears that the latter is caused by the influence of meteorological factors with a diurnal period. Medvedev and Kulikov (2016) showed that the amplitude of the radiational harmonic S_1 in this part of the Black Sea can be significantly greater than the amplitudes of the gravitational diurnal harmonics O_1, P_1, and K_1 and is comparable with the M_2 amplitude.

One of the significant features of the Crimean (Feodosia, Yalta, and Sevastopol), the Caucasian (Gelendzhik, Tuapse, Sochi, Poti, and Batumi) and Turkish (Trabzon, Sinop, and Amasra) sea level spectra is a persistent spectral peak with a period almost exactly coinciding with the *inertial period*:

$$T_f = \frac{2\pi}{f} = \frac{2\pi}{2\Omega \sin\varphi} \approx \frac{11.967}{\sin\varphi} \approx 17 \text{ h } (1.41 \text{ cpd}), \quad (1)$$

where f is the Coriolis frequency, Ω is the frequency of the Earth rotation, and φ is the latitude of the observation site. On the Caucasian (Fig. 2b, d) and Turkish (Fig. 2f) coasts, it is more evident than on the Crimean coast (Fig. 2e). The inertial peak is a typical spectral feature of baroclinic open-ocean currents (cf.

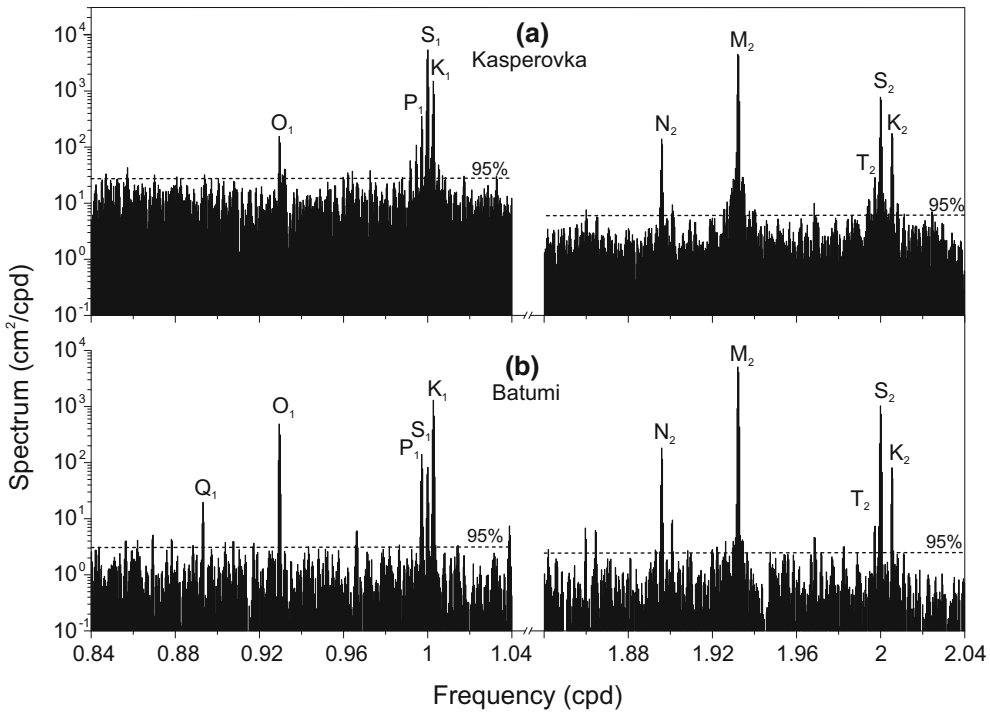

Figure 3
High-resolution sea level spectra in the Black Sea for diurnal and semidiurnal frequency bands at stations Kasperovka (**a**) and Batumi (**b**). Thin dashed lines show 95% confidence level for diurnal and semidiurnal harmonics calculated according to Chi-square distribution for each tidal band

LeBlond and Mysak 1978); however, it does not normally appear in the spectra of sea level oscillations which are presumably barotropic. The cause of this consistent peak in coastal sea level spectra in the Black Sea needs further research.

Important properties of diurnal and semidiurnal tides in the Black Sea can be identified based on high-resolution spectral analysis. Longterm series of tide gauge observations can provide the high-resolution spectra needed to split the diurnal and semidiurnal peaks into individual constituents (Munk and Cartwright 1966). As shown by Medvedev et al. (2013, 2017), Rabinovich and Medvedev (2015), and Medvedev and Kulikov (2016), this approach enables us to identify some specific features of the tidal formation which are indistinguishable in lower resolution spectra. In the present study, we conducted a detailed spectral analysis for long series with high-quality hourly observations at tide gauges Kasperovka (19 years, Dnieper Estuary) and Batumi (15 years, Caucasian coast). The length of the spectral KB-window for these series was 65 536 h, the spectral resolution was $\Delta f \approx 0.000366$ cpd, the number of degrees of freedom $v = 8$ for Kasperovka, and $v = 4$ for Batumi. The main attention was paid to the diurnal and semidiurnal frequency bands (Fig. 3). The major harmonics N_2, M_2, S_2, and K_2, as well as elliptical solar semidiurnal constituent T_2, are evident against the background noise in the semidiurnal tidal band, significantly exceeding the 95% confidence level (Fig. 3). The amplitude ratios for these harmonics approximately match the theoretical ratios for the tidal potential (Pugh and Woodworth 2014). Although the S_2 harmonic has both gravitational and radiational origin, the ratio of the magnitudes of the radiational/gravitational components varies from 0.05 to 0.6 in the Black Sea (Medvedev et al. 2016).

In the diurnal tidal band, the high-resolution spectral analysis revealed some interesting peculiarities. The "classical" ratio between major diurnal harmonics is observed at Batumi, but at Kasperovka the sea level spectrum (Fig. 3a) has some anomalous

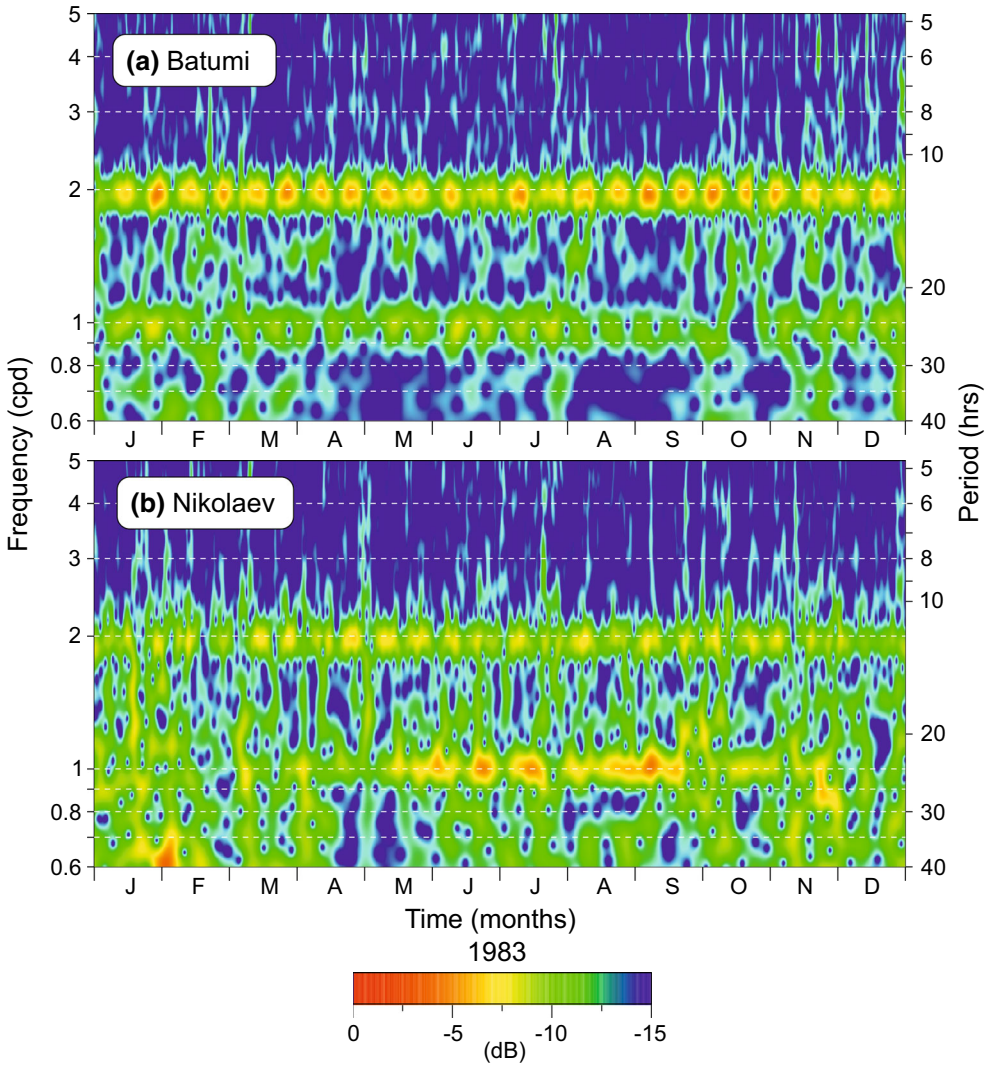

Figure 4
Frequency–time (*f*–*t*) wavelet diagrams of the sea level variability in frequency range 0.6–5 cpd in Batumi (**a**) and Nikolaev (**b**) in 1983

features: the Q_1 peak (well-defined at Batumi, see Fig. 3b) is absent, while the peak of the radiational harmonic S_1 is markedly strong higher than those of the gravitational harmonics O_1, P_1, and K_1. This proves the important role of meteorological factors in the formation of diurnal periodic sea level oscillations in the Dnieper Estuary.

To specify the spectral features of diurnal tides, we used the multiple-filter technique which is similar to wavelet analysis (e.g. Kulikov et al. 2004; Thomson and Emery 2014). Frequency–time (*f*–*t*) diagrams were constructed for the Batumi and Nikolaev tide gauges in the frequency range 0.6–5 cpy (Fig. 4). These stations were chosen because they have a different character of diurnal tidal sea level variability. The main signal in the Batumi *f*–*t* diagram (Fig. 4a) is a semidiurnal tide with fortnightly modulation of amplitude. The diurnal signal is weaker than the semidiurnal signal. The main feature of the diurnal signal at Batumi is the relative sustainability of its magnitude. In contrast¸ at Nikolaev (Fig. 4b), which is located at the head of the Bug Estuary, the magnitude of the diurnal signal varies strongly during the year. The maximum amplitude of diurnal tide is

observed in the summer period, and weaker diurnal sea level oscillations are observed in the winter period. This feature, apparently, is caused by the radiational origin of the diurnal tide in this area. The semidiurnal signal in the Nikolaev *f*–*t* diagram is similar to the corresponding signal in the Batumi *f*–*t* diagram. We conclude that the semidiurnal tides in both areas of the sea have an astronomical origin.

4. Harmonic Analysis of Tidal Oscillations

The clear prevalence of tidal harmonics in comparison to the background noise level allows applying the harmonic analysis for studying tides in the Black Sea. To calculate the tidal harmonic constants, we used the least squares method (Parker 2007). Based on the harmonic analysis, mean tidal amplitudes and Greenwich phase lags were calculated for 28 sites in the Black Sea. The calculations were based on high-quality yearly observations which do not have significant gaps in the records (Table 1). The results of calculations for individual years were vector averaged to obtain the mean multiyear values of amplitudes and phase lags (Medvedev et al. 2013, 2017). In total 66 tidal constituents were calculated and we selected the 9 largest harmonics: 5 diurnal (Q_1, O_1, P_1, S_1, and K_1) and 4 semidiurnal (N_2, M_2, S_2, and K_2). The results of the analysis are presented in Table 2.

The amplitudes of the major tidal harmonics differ significantly within the region. The M_2 amplitude in the Black Sea varies from 0.1 to 0.5 cm on the coast of the Crimean Peninsula, and from 0.7 to 0.9 cm on the coast of central Turkey to 3.4 cm in the northwestern part of the Black Sea (Odessa and Nikolaev). The S_2 amplitude varies from 0.1 cm near the Crimea to 1.8 cm in the northwestern part of the sea. A remarkable feature of semidiurnal tides is observed at Kherson: the amplitude of S_2 (2.9 cm) is almost twice the amplitude of M_2 (1.5 cm), while in the tidal potential (Pugh and Woodworth 2014) the ratio of the amplitudes H_{S_2}/H_{M_2} is 0.47. It appears that this anomaly is caused by the dominant influence of the radiational component in forming the overall harmonic S_2 in this region.

At Kherson, the highest amplitude of the radiational harmonic S_1 (5.6 cm) is observed, which is significantly higher than the amplitudes of the major gravitational harmonics O_1, K_1, and M_2 in the Black Sea. The amplitude of S_1 changes considerably from year to year because of its meteorological origin. According to the results of the harmonic analysis, the largest S_1 amplitude, 7.7 cm, was observed at Kherson in 1977. The longterm average S_1 amplitudes are also high at Kasperovka and Nikolaev: $\sim$ 4 cm, while on the Caucasian coast of the Black Sea, near the Crimea and the Danube Delta it is only 0.8–1.0 cm. The K_1 amplitude in the Black Sea varies from 0.1–0.3 cm at the Crimean coast and 0.2 cm at Sinop (Turkey), to 1.3 cm at Poti and Batumi, and to 1.5–1.8 cm in the Dnieper–Bug Estuary (Nikolaev, Stanislav, and Kasperovka). The O_1 amplitude is on average 0.2–0.4 cm, with the maximum at Poti and Batumi $\sim$ 0.8 cm. The mean P_1 amplitude in the Black Sea is 0.3–0.7 cm, with the maximum in the Dnieper–Bug Estuary up to 1.2 cm at Nikolaev and 0.8 cm at Stanislav. At these two stations, the P_1 amplitude is more than twice as large as the O_1 amplitude although their ratio in the tidal potential is $H_{P_1}/H_{O_1} \approx 0.47$. This anomaly is observed at all sites in the Dnieper–Bug Estuary. Within the estuary the N_2 amplitude is 0.2–0.6 cm, and the K_2 amplitude varies from 0.2 to 0.9 cm (Kherson), and Q_1 is less than 0.1 cm (Table 2).

The errors in the estimation of tidal amplitudes (ε_H) and phase lags (ε_G) were calculated using the following expressions (Pugh and Woodworth 2014):

$$\varepsilon_H = \sqrt{\frac{\sigma^2_{\Delta f}}{T \cdot \Delta f}}, \tag{2}$$

$$\varepsilon_G = \frac{1}{H}\sqrt{\frac{\sigma^2_{\Delta f}}{T \cdot \Delta f}} = \frac{\varepsilon_H}{H} \text{ (in radians)},$$

where $\sigma^2_{\Delta f}$ is the background noise variance in the frequency band Δf (diurnal or semidiurnal), T is the series length used for the harmonic analysis (in this study $T = 1$ year), and H is the amplitude of the corresponding tidal harmonic. As evident from Eq. (2), the amplitude error has one absolute value for all harmonics in a given frequency band, while the phase lag becomes larger for a lower amplitude.

Table 2

Mean amplitudes (H) and Greenwich phase lag (G) of fundamental tidal harmonics, the form factor (F), and maximum tidal range (R) at various stations in the Black Sea H and G of fundamental tidal harmonics for Burgas and Varna were obtained from (Ivanov 2015)

Station	Q_1		O_1		P_1		S_1		K_1		N_2		M_2		S_2		K_2		F	R (cm)
	H (cm)	G (°)	H (cm)	G (°)	H (cm)	G (°)	H (cm)	G (°)	H (cm)	G (°)	H (cm)	G (°)	H (cm)	G (°)	H (cm)	G (°)	H (cm)	G (°)		
Bolshoe (1)	0.09	68	0.34	89	0.07	23	0.53	195	0.44	71	0.18	90	0.97	88	0.39	109	0.15	100	0.57	4.4
Vilkovo (2)	0.15	90	0.31	87	0.17	42	0.40	207	0.44	81	0.20	108	1.04	108	0.48	122	0.16	115	0.49	4.7
Prorva (3)	0.15	71	0.42	72	0.08	47	0.40	180	0.58	75	0.31	82	1.65	88	0.76	102	0.25	96	0.41	7.0
Belgorod-Dnestrovskiy (4)	0.05	158	0.23	129	0.33	117	0.75	342	0.58	138	0.09	152	0.50	158	0.31	169	0.08	180	1.00	4.5
Paromnaja Pereprava (5)	0.09	57	0.48	66	0.43	43	0.91	238	0.88	70	0.58	89	3.30	90	1.77	99	0.54	93	0.27	13.6
Illichivsk (6)	0.11	57	0.47	66	0.32	42	0.59	233	0.86	64	0.56	77	3.28	78	1.75	87	0.56	83	0.26	13.2
Odessa (7)	0.13	67	0.46	68	0.38	39	0.88	243	0.93	63	0.58	78	3.44	79	1.85	86	0.57	81	0.26	14.1
Ochakov (8)	0.05	87	0.28	109	0.44	61	1.51	312	0.72	113	0.27	110	1.57	107	0.97	115	0.26	101	0.39	9.1
Heroyskoe (9)	0.04	150	0.31	121	0.53	82	2.32	316	0.96	133	0.24	190	1.50	188	0.77	181	0.22	191	0.56	9.9
Nikolaev (10)	0.06	190	0.54	148	1.17	79	4.15	321	1.81	140	0.56	259	3.39	265	1.47	267	0.46	279	0.48	18.9
Stanislav (11)	0.09	215	0.59	146	1.04	105	3.24	294	1.55	113	0.58	204	2.75	204	1.22	205	0.48	224	0.54	15.8
Kasperovka (12)	0.05	182	0.46	135	0.68	70	4.01	304	1.50	133	0.46	213	2.72	219	1.14	240	0.51	238	0.51	15.8
Kherson (13)	0.04	153	0.36	179	0.71	300	5.63	300	1.27	188	0.26	278	1.55	281	2.92	295	0.87	262	0.36	19.2
Sevastopol (14)	0.02	352	0.11	25	0.19	3	0.61	197	0.30	36	0.08	54	0.41	46	0.23	25	0.05	40	0.64	2.7
Yalta (15)	0.01	342	0.04	330	0.06	286	0.37	178	0.12	334	0.03	153	0.13	144	0.05	342	0.01	170	0.91	1.1
Feodosia (16)	0.03	240	0.15	254	0.19	346	0.72	213	0.17	311	0.10	179	0.53	183	0.23	209	0.05	184	0.41	3.1
Gelendzhik (17)	0.12	239	0.38	239	0.13	251	0.31	180	0.53	240	0.24	204	1.20	203	0.49	212	0.15	206	0.54	5.3
Tuapse (18)	0.11	251	0.51	244	0.28	249	0.46	196	0.77	247	0.31	210	1.58	211	0.78	217	0.22	216	0.54	7.6
Sochi (19)	0.14	236	0.60	246	0.34	259	0.54	223	0.86	253	0.32	221	1.72	223	0.78	225	0.23	221	0.59	8.6
Kulevi (20)	0.25	187	0.56	230	0.32	257	0.96	235	1.30	260	0.43	224	2.37	243	1.04	245	0.42	253	0.55	10.9
Poti (Rioni) (21)	0.35	119	0.53	296	0.28	262	0.62	225	1.08	266	0.42	236	1.70	255	0.81	254	0.11	306	0.64	9.0
Poti (22)	0.15	249	0.79	244	0.44	249	0.23	234	1.29	252	0.47	225	2.33	227	0.95	236	0.28	231	0.64	11.1
Batumi (23)	0.16	245	0.85	237	0.40	244	0.55	198	1.29	240	0.51	215	2.75	217	1.23	224	0.35	215	0.54	12.5
Trabzon (24)	0.12	241	0.65	238	0.32	255	0.16	215	0.93	238	0.43	225	2.27	227	1.06	233	0.30	232	0.47	10.1
Sinop (25)	0.06	125	0.17	240	0.04	221	0.37	30	0.20	205	0.14	243	0.69	241	0.34	252	0.09	258	0.36	3.1
Amasra (26)	0.02	33	0.29	63	0.35	57	0.81	298	0.71	73	0.16	7	0.86	3	0.55	36	0.14	12	0.71	5.8
Şile (27)	0.11	80	0.52	71	0.32	37	0.54	217	0.83	61	0.35	27	1.73	24	0.79	28	0.22	28	0.54	8.5
Iğneada (28)	0.17	64	0.77	72	0.38	86	0.24	321	0.99	80	0.40	34	2.19	33	1.09	40	0.25	40	0.54	10.5
Burgas (29)	0.25	68	0.82	65	0.72	90	–	–	1.56	77	0.40	20	2.13	28	1.08	30	0.69	11	0.74	–
Varna (30)	–	–	0.81	52	0.97	67	–	–	1.84	63	0.40	5	1.90	10	1.02	11	0.53	336	0.91	–

According to the spectral analysis, the variance values for Kasperovka $\sigma^2_{\Delta f}(1) = \Delta f \times \hat{S}_x(1) = 2.95\ \mathrm{cm}^2$ for the diurnal band and $\sigma^2_{\Delta f}(2) = \Delta f \cdot \hat{S}_x(2) = 0.61\ \mathrm{cm}^2$ for the semidiurnal band, where $\hat{S}_x(1,2)$ is the mean spectral value for the corresponding band (Fig. 3a), while $\Delta f = 0.2$ cpd is the bandwidth. The corresponding variance values for Batumi are smaller: $\sigma^2_{\Delta f}(1) = 0.14\ \mathrm{cm}^2$ and $\sigma^2_{\Delta f}(2) = 0.06\ \mathrm{cm}^2$ (Fig. 3b). Calculated errors for the diurnal amplitudes at these stations are $\varepsilon_H(1) = 0.20$ cm (Kasperovka) and 0.06 cm (Batumi); errors for the semidiurnal amplitudes are $\varepsilon_H(2) = 0.09$ cm and 0.05 cm, respectively.

The phase lag error (ε_G) is inversely proportional to the harmonic amplitude. These errors are (based on the data from Table 2): 8° (K_1), 25° (O_1), 2° (M_2), and 5° (S_2) for Kasperovka; and 3° (K_1), 4° (O_1), 1° (M_2), and 2° (S_2) for Batumi. The errors in amplitudes and phase lags for other stations, in general, are similar to those for Kasperovka and Batumi. Thus, the errors are relatively smaller compared to the calculated amplitudes and phase lags.

The harmonic constants calculated for various years were used to estimate the scatter and errors of specific harmonics for individual stations. The M_2 amplitude changes very little over time: the error in amplitude is from 3–5 to 12–15% for tide gauges Bolshoe, Prorva, and Kherson. Depending on the station, the phase-lag error for M_2 varies from 2° to 7°. The S_2 amplitude error changes from 6 to 17% and the phase-lag error from 7° to 11°. For K_1 the amplitude error is from 8 to 20%, while for O_1 is up to 10–45% of its value. The phase-lag scatter for K_1 is 5°–12°, and for O_1 it is 15°–25°. The averaging of estimated amplitudes and phase lags over a large number of years enables us to determine their accuracy which improves as $1/\sqrt{n}$, where n is the number of independent yearly series used for the calculations. In general, these accuracy estimations are very close to the error estimates obtained from the spectral analysis (2).

5. Numerical Modelling of Tides

To understand the formation mechanisms of tides in the Black Sea, we need to know the tidal spatial structure. The results of the harmonic analysis of tide gauge data enable us to examine specific tidal features along the coast, but not in the open part of the Black Sea. Numerical modelling provides an effective method to evaluate tides over the entire sea basin, and in combination with actual observations, describe the tidal dynamics and particular physical properties of tides in the sea as a whole and in specific regions.

The barotropic tides are usually simulated using 2D models based on the momentum equations in the long-wave approximation. In the present study we used the 2D version of the Princeton Ocean Model (POM) (Mellor 2004); the same model has been used previously by Kulikov et al. (2015) for the numerical modelling of sea level variability in the Baltic Sea. The forcing in the momentum equations was specified through the gradients of the tidal potential fields over the Black Sea:

$$\vec{F}_T = -(1 + k - h)\nabla\overline{\Omega}, \tag{3}$$

where $k = 0.3$ and $h = 0.61$ are the Love numbers, $\overline{\Omega}$ is the tidal potential that was calculated for spherical harmonics via the formulas provided by Munk and Cartwright (1966). Also, our numerical model included the tidal loading potential obtained from FES2014 (Finite Element Solution tidal model) produced by NOVELTIS, LEGOS, and CLS Space Oceanography Division and distributed by AVISO, with support from CNES (http://www.aviso.altimetry.fr/).

The energy dissipation of generated flows is caused by the vertical turbulent viscosity. The friction force in the momentum equations is determined by the speed of the bottom flow and the friction coefficient:

$$(\tau_{bx}, \tau_{by}) = (C_b u_b|\vec{\mathbf{u}}_b|, C_b v_b|\vec{\mathbf{u}}_b|), \tag{4}$$

where $\vec{\mathbf{u}}_b = (u_b, v_b)$ is the flow velocity above the bottom boundary layer (that assumed to be equal to the barotropic velocity $\vec{\mathbf{u}}$ for the 2D model), C_b is the bottom friction coefficient which has following form:

$$C_b = \mathrm{Max}\left[\frac{\kappa^2}{(\ln\{0.5H/z_0\})^2},\ 0.0025\right] \tag{5}$$

where $\kappa = 0.4$ is the von Kármán constant, $z_0 = 0.01$ m is the bed roughness length. A minimum

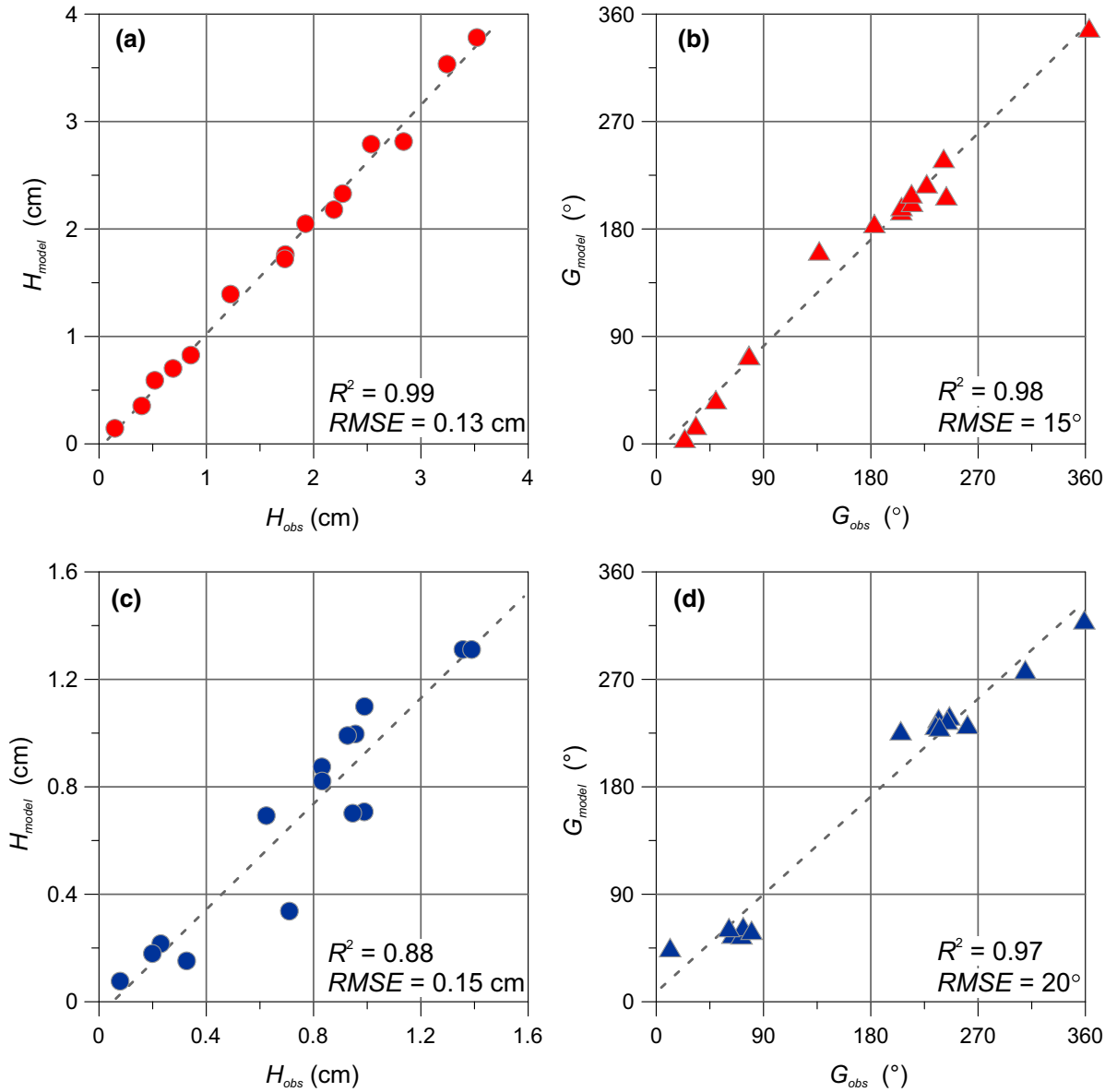

Figure 5
The comparison of amplitudes (**a**, **c**) and phase lags (**b**, **d**) of harmonics M_2 (**a**, **b**) and K_1 (**c**, **d**) estimated by results of the numerical modelling (H_{model} and G_{model}) and tide gauge observations (H_{obs} and G_{obs})

value for the bottom friction coefficient, C_b= 0.0025, was applied to avoid having the bottom drag effect vanish when the water depth is very large.

The GEBCO Black Sea bathymetry with spatial resolution of 30 arcseconds was used to create a grid with a constant step in latitude and longitude: $\Delta x = 1'$ and $\Delta y = 1'$. The Bosphorus entrance was closed. As a result of the numerical simulation, the tidal sea level variations were reproduced for the year 1978. This year had the largest number of high-quality tide gauge records in the Black Sea, and these records were used to verify the model.

The verification was conducted by comparing the numerically computed and observed amplitudes and phase lags of the M_2 and K_1 constituents for 15 reference stations located in various parts of the Black

Sea: Illichivsk, Odessa, Sevastopol, Yalta, Feodosia, Gelendzhik, Tuapse, Sochi, Poti, Batumi, Trabzon, Sinop, Amasra, Şile, and Iğneada. The results of this comparison demonstrate that the constructed model values for both semidiurnal (Fig. 5a, b) and diurnal (Fig. 5c, d) tides are in good agreement with the observations. For semidiurnal tides, the coefficient of determination $R^2 = 0.98–0.99$ both for amplitudes and phase lags; the root mean square error, RMSE= 0.13 cm for amplitudes and 15° for phase lags; for diurnal tides $R^2 = 0.88$ for amplitudes, $R^2 = 0.97$ for phase lags, RMSE= 0.15 cm for amplitudes, and 20° for phase lags.

According to the observations, the semidiurnal tides in the Black Sea are determined by an amphidromic system with clockwise rotation, and the model correctly reproduces this feature (Fig. 6a). There are very few places in the Northern Hemisphere, as in the Black Sea, that have clockwise M_2 amphidromic systems: the Gulf of Tonkin in the South China Sea, the Gulf of Thailand in the marginal part of the western Pacific Ocean, and the Gulf of Martaban in the northern part of the Andaman Sea (cf. Egbert and Erofeeva 2002; see details here: http://volkov.oce.orst.edu/tides/global.html). However, in each of these locations, tides are co-oscillating, i.e. generated by tidal waves incoming from external basins. The uniqueness of the clockwise M_2 amphidromic system in the Black Sea is that this basin is closed, so tides there are independent ("forced").

Harris (1897–1907) explained that such systems are formed by the superposition of two standing waves crossing at some angle on which the direction of rotation depends. Sterneck (1922) assumed that the tidal forces act synchronously upon the entire water mass of the Black Sea and that the actual semidiurnal tides in this sea are formed by superposition of four oscillations: (1) the west–east and (2) north–south oscillations caused directly by the corresponding components of tide-generating forces; (3) the north–south, and (4) west–east oscillations caused by the action of the Coriolis forcing on the oscillations (1) and (2), respectively.

The amphidromic point of this system is located to the south of the Crimean Peninsula, and as a result, the minimum of the M_2 amplitude is observed there. As correctly pointed out by Fomicheva et al. (1991),

Figure 6 ▶
Tidal maps of amplitudes (shaded) and co-tidal lines (solid lines) in degrees of (**a**) semidiurnal harmonic M_2 and (**b**) diurnal harmonic K_1 in the Black Sea according to the numerical modelling. The results of harmonic analysis of tide gauge observations are placed near the corresponding sites, the amplitude is in the numerator (red regular font) and the phase lag is in the denominator (black italic font). Green dots are the Bulgarian tide gauges. The results of harmonic analysis for these tide gauges were obtained from (Ivanov 2015). Map of the maximal tidal range (**c**) in the Black Sea. Co-range lines are shown by solid lines

the semidiurnal tides in the western and eastern parts of the sea are in almost antiphase. In the northwestern part of the sea, the semidiurnal tide has a complex structure, which in earlier studies (Defant 1961; Engel 1974; Fomicheva et al. 1991) was not reproduced due to the limited observational data and insufficient possibilities for numerical simulations. The results of the present study indicate that in the shallow northwestern part of the Black Sea, a degenerate (virtual) amphidromic M_2 system is formed (Fig. 7a). At Odessa and Illichivsk the amplitude of the harmonic M_2 is 3.3 cm and the phase $\sim 78°$ (Table 2). At Ochakov and at Heroyskoe, which are located at the entrance of the Dnieper–Bug Estuary, the M_2 amplitude decreases to 1.5 cm, and the phase lag increases rapidly as the M_2 tide propagates into the estuary: up to 107° at Ochakov and 188° at Heroyskoe. Moving deep into the Dnieper–Bug Estuary the M_2 amplitude increases up to 3.4 cm at Nikolaev and 2.7 cm at Kasperovka. The phase lag at the head of the estuary reaches 260–280°, thus the M_2 tidal oscillations in this area are in antiphase relative to the M_2 tides in Odessa and Illichivsk (78°). The maximum M_2 amplitudes of 4.5 cm are calculated to be in Karkinit Bay (the western coast of the Crimea) (Fig. 7a). Unfortunately, there are no hourly tide gauge observations in this bay. However, our modelling results for this region are in good agreement with those of Zalesny et al. (2016) who also found that the maximum amplitudes of the semidiurnal tide are in Karkinit Bay.

In contrast to the semidiurnal tides, the diurnal tides have a counterclockwise rotating amphidromic system located in the central part of the Black Sea (Fig. 6b). Diurnal tidal sea level oscillations in the western and eastern parts of the sea are also in antiphase, the phase contrast is close to 180°. For K_1, the

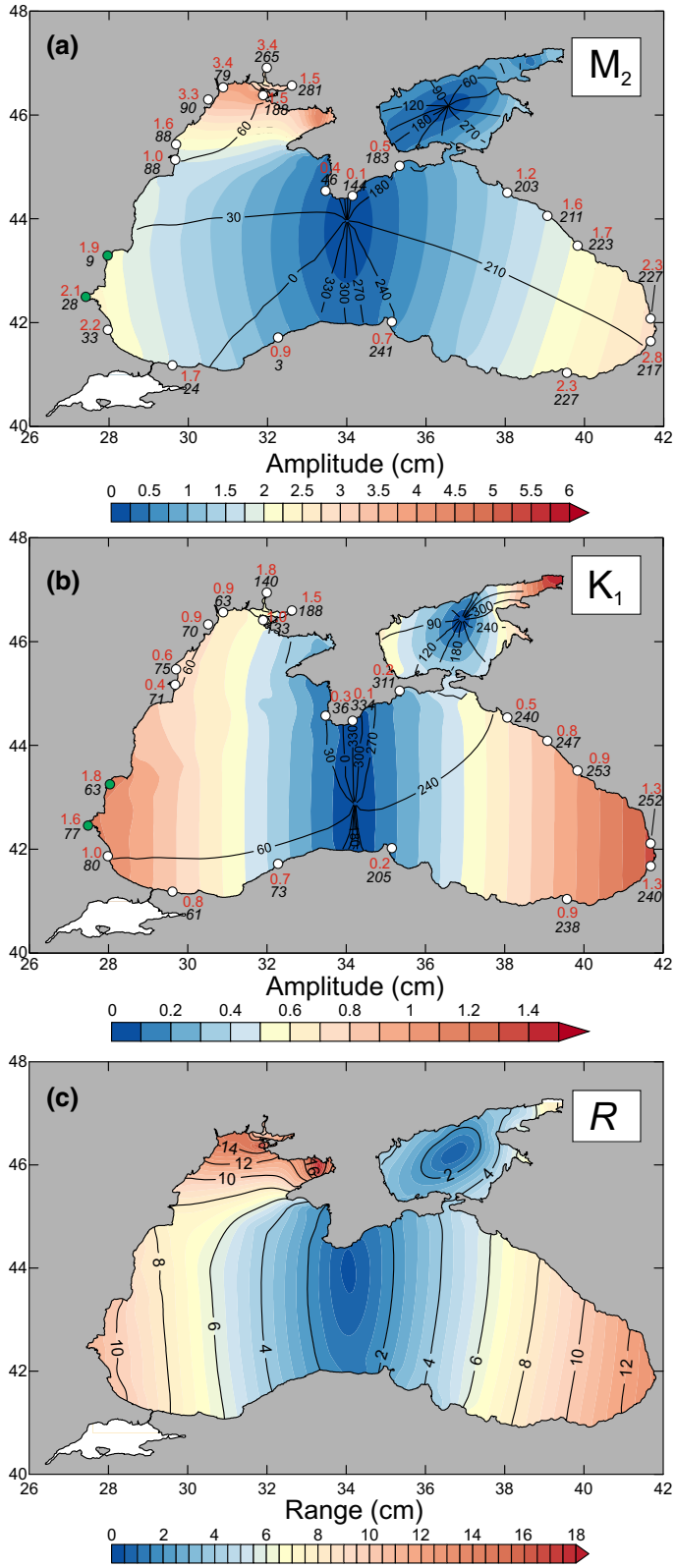
(a)
M2
Amplitude (cm)
0 0.5 1 1.5 2 2.5 3 3.5 4 4.5 5 5.5 6
(b)
K1
Amplitude (cm)
0 0.2 0.4 0.6 0.8 1 1.2 1.4
(c)
R
Range (cm)
0 2 4 6 8 10 12 14 16 18
26 28 30 32 34 36 38 40 42
40 42 44 46 48

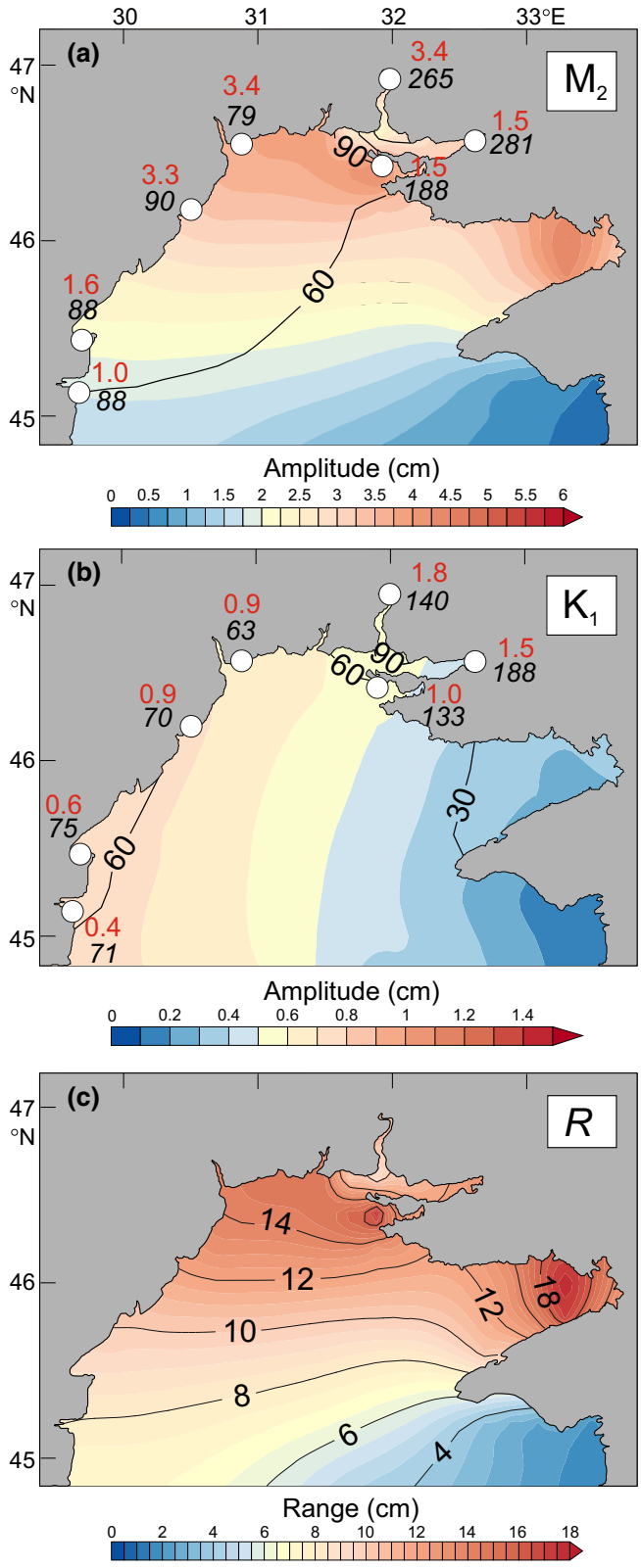
30
31
32
33°E
47
°N
46
45
(a)
M2
3.4
265
3.4
79
1.5
281
90
1.5
188
3.3
90
60
1.6
88
1.0
88
Amplitude (cm)
0 0.5 1 1.5 2 2.5 3 3.5 4 4.5 5 5.5 6
(b)
K1
1.8
140
0.9
63
90
60
1.5
188
0.9
70
1.0
133
30
0.6
75
60
0.4
71
Amplitude (cm)
0 0.2 0.4 0.6 0.8 1 1.2 1.4
(c)
R
14
12
10
8
6
4
12
18
Range (cm)
0 2 4 6 8 10 12 14 16 18

◀Figure 7
Tidal maps of amplitudes (shaded) and co-tidal lines (solid lines) in degrees of (**a**) semidiurnal harmonic M_2 and (**b**) diurnal harmonic K_1 in the northwestern part of the Black Sea according to the numerical modelling. Map of the maximal tidal range (**c**) in the northwestern part of the Black Sea. Co-range lines are shown by solid lines

phase lag differences between the north and south ends of the east coast are 13°, similar to M_2 semidiurnal harmonic, i.e. the diurnal sea level flood tide occurs almost simultaneously for the entire eastern coast of the Black Sea. On the opposite, west coast of the sea, the K_1 phase difference is also small; e.g. between Vilkovo and Odessa it is only 12°. On the coast of the Crimean Peninsula, there are abrupt changes in phase and small K_1 amplitudes which are caused by the proximity of the amphidromic point. In the Dnieper–Bug Estuary (Fig. 7b), a rapid increase in amplitudes (from 0.9 to 1.8 cm) and phase lag (from 63° to 188°) for harmonic K_1 is observed (based on results of harmonic analysis of tide gauge observations). In the results of numerical modelling, the maximum amplitude of the harmonic K_1 in the Dnieper–Bug Estuary is 0.6–0.7 cm. This difference between observation and model amplitudes may be caused by the influence of radiational tides in this estuary. The present numerical model did not take into account the radiational effects in sea level oscillations. In general, the results of numerical modelling (Fig. 6b) indicate that the maximum amplitude of the diurnal harmonic K_1 on the eastern coast of the Black Sea (1.3 cm at Poti and Batumi) is in good agreement with the actually observed amplitudes at these two stations.

According to the results of our numerical modelling, diurnal and semidiurnal tides in the Sea of Azov are determined by "classical" amphidromic systems, both rotating counterclockwise, with M_2 and K_1 amphidromic points located in the central part of the sea (Figs. 6a, b). The maximum M_2 amplitudes of 1.1–1.3 cm are observed in the eastern part of the Sea of Azov near Primorsko-Akhtarsk and in Taganrog Bay. The maximum K_1 amplitude of 1.4 cm is observed in the head of Taganrog Bay. The main eigen mode of this sea has a period of about 24 h (Defant 1961); therefore, a resonant amplification of diurnal tides in the Sea of Azov is observed.

The numerical results obtained in the present study can substantially improve upon existing tidal charts by Defant (1961) and Engel (1974). The co-tidal chart in the book of Defant (1961) was based on the results at the beginning of the twentieth century by Sterneck (1922). Engel (1974) calculated the M_2 co-tidal chart by means of the Hansen numerical hydrodynamic model. Friction, the Earth's rotation, and the real Black Sea bathymetry and shape were taken into account, but the spatial resolution of the model was poor ($\sim$ 1/3°), a number of important topographic and coastal features were not resolved and the author (Engel 1974) did not have reliable observational data to fit and verify the model. From this point of view, the tidal charts constructed as part of the current study are a significant advancement in the general understanding of the Black Sea dynamics. Two new elements of these charts are probably the most important: (1) computed tidal charts for the Sea of Azov and (2) modelled tides for the northwestern part of the sea, including the Dnieper–Bug Estuary.

6. *Nonharmonic Tidal Constituents*

Constants obtained from harmonic analysis were used to calculate the type and heights of tidal sea level oscillations in the Black Sea. The type of tides ("form factor") is traditionally determined by the ratio of major diurnal and semidiurnal harmonics (Pugh and Woodworth 2014):

$$F = \frac{H_{K_1} + H_{O_1}}{H_{M_2} + H_{S_2}}. \tag{6}$$

Typical values of F in the Black Sea vary from 0.3 (Odessa, Illichivsk) to 0.5–0.6 (east coast, the Dnieper–Bug Estuary, the Danube Delta, and the Crimean Peninsula coast). These F values correspond to a mixed mainly semidiurnal type of tide ($0.25 < F < 1.5$). The value of F in most of the Sea of Azov is 0.6–1.5. In Taganrog Bay, F reaches 2.5, which corresponds to a mixed mainly diurnal type ($1.5 < F < 3$).

However, the results of our study show that the ratio (6) for some areas of the Black Sea did not completely reflect the real nature of the tidal sea level oscillations due to the absence of the S_1 harmonic amplitude in the expression (6). The S_1 harmonic

amplitude is significantly larger than any other gravitational harmonic in the Dnieper–Bug Estuary. We calculated the ratio of the amplitude of the S_1 harmonic to the sum of the amplitudes of the O_1 and K_1 harmonics. For the eastern coast of the Black Sea, the value of this ratio is 0.3–0.4, on the western coast of the sea this value is 0.5–0.7. However, in the northwestern part of the sea this value is significantly greater: in Ochakov this ratio is 1.5, in Nikolaev it is 1.8, and in Kherson it is 3.5.

The results of harmonic analysis allow us to estimate the tidal range (Table 2). We used the harmonic tidal constants for diurnal (including S_1), semidiurnal and shallow water constituents to predict tidal sea levels along the coasts of the Black Sea for 19 years. Tidal range was calculated as the maximum range of tidal sea level oscillations during one lunar day ($\sim$ 25 h). A maximum tidal range (R) of 18.9 cm is observed at Nikolaev in the estuary of the Southern Bug River, and of 19.2 cm at Kherson in the estuary of the Dnieper River. Inside the Dnieper–Bug estuaries R is 15.8 cm, and at Odessa and Illichivsk R is 13–14 cm. On the east coast, R varies from 5.3 cm at Gelendzhik to 12.6 cm at Batumi. The smallest tidal range of 1.1 cm is observed at Yalta, the southern coast of the Crimean Peninsula.

The tidal range in the Black Sea was evaluated based on the results of numerical modelling (Fig. 6c). The calculations were done in the same way as described above, but without the S_1 contribution, because this harmonic has radiational (not gravitational) origin and had not been simulated in the numerical experiments. The maximum tidal ranges (R) estimated from the numerical model results are in Karkinit Bay and Yahorlyk Bay, 18 and 17.5 cm, respectively, (Fig. 7c). On the east coast of the sea (near Batumi) R is 13 cm, on the west coast (near Burgas) R is 10.7 cm. The smallest R of 1.0 cm is on the southern coast of the Crimean Peninsula. The maximum R in the Sea of Azov is located in the head of Taganrog Bay and amounts to 8 cm (Fig. 6c).

7. Discussion

The amplitudes and phase lags of the major tidal harmonics estimated in the present study are in agreement with the results of other authors (Engel 1974; Fomicheva et al. 1991). The obtained tidal constants allowed us to clarify the spatial structure of the amplitudes and phase lags of major tidal harmonics in the northwestern part of the Black Sea. The sea level observational data for the Dnieper–Bug Estuary have not been examined before and have not been used to construct tidal charts (cf. Defant 1961; Engel 1974; Fomicheva et al. 1991; Goryachkin and Ivanov 2006).

Our estimates of the maximum tidal range differ significantly from those presented by Fomicheva et al. (1991) and Goryachkin and Ivanov (2006). This disagreement is mainly caused by two factors: (1) the number of harmonics used to estimate the tidal range (in this study we applied a larger quantity of semidiurnal and diurnal harmonics, including the radiational harmonic S_1); (2) the spatial and temporal coverage is more detailed in comparison with other research papers. In particular, in previous studies (Fomicheva et al. 1991; Goryachkin and Ivanov 2006) they did not consider stations Nikolaev, Kasperovka, and Kherson, located in the Dnieper–Bug Estuary, where the maximum tidal range, up to 19 cm, was found.

The spectral and harmonic analyses of the long series of observations revealed an important role of radiational tides in forming the diurnal oscillations in the northwestern part of the sea. At stations Kherson, Nikolaev, Kasperovka, and Heroyskoe the amplitude of the radiational harmonic S_1 is greater than any of the harmonics for the astronomical tide, including M_2 and K_1. It appears that the K_1 and P_1 peaks, evident in sea level spectra at these stations, are caused not only by gravitational tides, but also by radiational factors, in particular by sea breezes. For example, Rabinovich and Medvedev (2015) showed that harmonic satellites with K_1 and P_1 frequencies may be generated by the seasonal modulation of the major diurnal radiational harmonic S_1. This modulation can be caused by various hydrometeorological reasons including ice cover, river runoff, seasonal changes of cloudiness, etc.

In general, the amplitude of the diurnal radiational harmonic S_1 in the Black Sea does not exceed 1 cm, except in the Dnieper–Bug Estuary where the amplitude of the harmonic increases up to 4–6 cm.

Thus, at Nikolaev located at the estuary of the Southern Bug River, the S_1 amplitude is 4.1 cm and at Kherson (Dnieper River Estuary) 5.6 cm. Near the Danube Delta (Vilkovo, Bolshoe and Prorva) the S_1 amplitude is 0.4–0.5 cm. Apparently, the increase of the S_1 amplitude in the Dnieper–Bug Estuary is caused by the combined effect of the shallow water (mean depth is 6–7 m), the estuary isolation (the lagoon is connected with the sea by a strait with a width of 3.6 km), and strong sea breezes which are the driving factors influencing diurnal sea level oscillations.

In recent decades significant progress has been achieved in improving global barotropic tide models. This progress has been helped by the available satellite altimetry. In Stammer et al. (2014), the detailed comparison of the main modern global barotropic tide models is presented. Some of these models include the Black Sea. In our study, we examined the TPXO8 model of Oregon State University (Egbert and Erofeeva 2002) and the FES2014 model. In general, the co-tidal charts from these models for the Black Sea are very close to our numerical modelling results. In future, a detailed comparison of these models will be carried out.

8. Conclusions

In the present study, tidal sea level oscillations in the Black Sea were examined based on long series of hourly sea level observations. In general, our findings can significantly clarify and extend the results of previous studies of the Black Sea tides (cf. Endrös 1932; Defant 1961; Engel 1974; Fomicheva et al. 1991). High-quality longterm tide gauge data that were used in the present study allowed us: (1) to calculate the harmonic constants for more stations and with much higher accuracy than it was previously possible; (2) to separate harmonics belonging to one group, in particular, S_2 and K_2 and P_1, S_1, and K_1. For a "non-tidal" basin such as the Black Sea, these were especially important because it enabled us to divide gravitational and radiational tides and to estimate the relative influence of the latter.

The results of high-resolution spectral analysis showed discrete tidal peaks corresponding to the major, secondary diurnal, and semidiurnal tidal harmonics. We used harmonic analysis to calculate the tidal harmonic constants at 28 stations for individual years and then vector averaged them to estimate mean multiyear values of amplitudes and phase lags. The results of this analysis indicate that semidiurnal tides prevail over diurnal tides on the east and west coasts of the Black Sea, while in the central part of the sea, near the Crimean Peninsula, both types of tides were approximately equal and weak.

The numerical modelling allowed us to reconstruct the spatial structure of the diurnal and semidiurnal tides in the Black Sea. Although the amphidromic systems for the diurnal and semidiurnal tides look alike, they rotate in the opposite directions: counterclockwise and clockwise, respectively. Amphidromic points for both systems are located near the Crimean Peninsula, so in this part of the sea, there are minimum amplitudes of harmonics K_1 and M_2 (0.1 cm at Yalta). Tides in the western and eastern parts of the sea are in antiphase. Along the eastern coast the semidiurnal tides oscillate almost synchronously: the phase lag differences between Gelendzhik and Batumi are only $\sim 14°$. Maximum amplitudes of 4.5 cm for harmonic M_2 were found from observations at Karkinit Bay (based on the results of the numerical modelling) and up to 3.2 cm at Odessa.

The maximum tidal range in the Black Sea varies from 1.1 cm near the Crimean Peninsula to 19 cm in the Dnieper–Bug Estuary (Nikolaev and Kherson), 13–14 cm at Odessa, and Illichivsk and up to 12.6 cm on the east coast of the Black Sea (Batumi). In general, the semidiurnal tides prevail in the Black Sea. The radiational tides make an important contribution to the formation of the maximum tidal range in the Dnieper–Bug Estuary. At Nikolaev (the estuary of the Southern Bug River) the amplitude of S_1 is 4.1 cm, at Kherson (the mouth of the Dnieper River) 5.6 cm.

Acknowledgements

The author would like to thank Evgueni Kulikov, Alexander Rabinovich, Alisa Medvedeva (all from P.P. Shirshov Institute of Oceanology, Moscow, Russia), and Alena Sokolyanskaya for useful

discussions and helpful comments. Also, the author gratefully acknowledges Fred Stephenson (Institute of Ocean Sciences, Sidney, BC, Canada), Philip Woodworth (National Oceanography Centre, Liverpool, UK), and Svetlana Erofeeva (COAS, Oregon State University, Corvallis, Oregon, USA) for their very interesting and constructive comments. The results of Sect. 6 were obtained in the framework of the State assignment of FASO Russia (Theme no. 0149-2018-0015). The studies presented in Sects. 3 and 4 were supported by the RFBR grant (Project no. 16-35-60071) and in Sect. 5 by the RSF grant (Project no. 14-50-00095).

References

Alpar, B., & Yüce, H. (1998). Sea-level variations and their interactions between the Black Sea and the Aegean Sea. *Estuarine, Coastal and Shelf Science, 46*(5), 609–619.

Book, J. W., Jarosz, E., Beşiktepe, Ş, & Cambazoğlu, M. K. (2010). Observations of tidal energy and tidal fluxes through the Turkish Straits System. *EGU General Assembly Conference Abstracts, 12*, 5634. http://meetingorganizer.copernicus.org/EGU2010/EGU2010-5634.pdf.

Defant, A. (1961). *Physical oceanography* (Vol. II). Oxford: Pergamon Press.

Egbert, G. D., & Erofeeva S. Y. (2002). Efficient inverse modeling of barotropic ocean tides. *Journal of Atmospheric and Oceanic Technology, 19*(2), 183–204. https://doi.org/10.1175/1520-0426(2002)019<0183:eimobo>2.0.co;2.

Endrös, A. (1932). Die Seiches des Schwarzen und Asowschen Meeres und die dortigen Hubhöhen der Gezeiten. *Annalen der Hydrographie Maritimen Meteorologie, 60,* 442–453.

Engel, M. (1974). Hydrodynamish-numerische Ermittlung von Bewegungsvorgängen im Schwarzen Meer. *Mitteilungen des Instituts für Meereskunde der Universität Hamburg, 22,* 1–72.

Fomicheva, L. A., Rabinovich, A. B., & Demidov, A. N. (1991). The sea level (in Russian). In: *The Project "Seas of the Soviet Union." Hydrometeorology and Hydrochemistry of Seas of Soviet Union, Vol. 4: The Black Sea. No. 1* (329–354) St. Petersburg: Gidrometeoizdat.

German, V Kh. (1970). Spectral analysis of water level oscillations in the Azov, Black, and Caspian seas within the range from one cycle over few hours until one cycle over few days (in Russian). *Proceedings of State Oceanographic Institute, 103,* 52–73.

Goryachkin, Yu N, & Ivanov, V. A. (2006). *The Black Sea level: Past, present, and future*. Sevastopol: Marine Hydrophysical Institute, National Academy of Sciences of Ukraine. **(in Russian)**.

Harris, R. A. (1897–1907). *Manual of tides: appendices to reports of the U.S. coast and geodetic survey*. Washington, DC: Government Printing Office.

Ivanov, A. I. (2015). Harmonic analysis of tide gauge data 2013–2014 in Bulgaria. *Bulgarian Chemical Communications, 47,* 343–348.

Ivanov, V. A., & Yastreb, V. P. (1989). Fluctuations of the Black Sea level. *Water Resources, 16*(2), 173–179.

Krsteva, E. (1981). Diurnal amplitudes of changes of the Black Sea level near Varna and Burgas (in Bulgarian). *Problemi na Geographiata (Bulgarian), 2,* 15–24.

Kulikov, E. A., Fain, I. V., & Medvedev, I. P. (2015). Numerical modeling of anemobaric fluctuations of the Baltic Sea level. *Russian Meteorology and Hydrology, 40*(2), 100–108.

Kulikov, E. A., Rabinovich, A. B., & Carmack, E. C. (2004). Barotropic and baroclinic tidal currents on the Mackenzie shelf break in the southeastern Beaufort Sea. *Journal of Geophysical Research—Oceans, 109,* C05020. https://doi.org/10.1029/2003jc001986.

Kurchatov, I. V. (1925). Seiches in the Black and Azov seas (in Russian). *Izvestia Tsentralnogo Gidromet Byuro, 4,* 149–158.

LeBlond, P. H., & Mysak, L. (1978). *Waves in the ocean*. New York: Elsevier.

Maramzin, V. Ya. (1985). Calculation of seiche oscillations by finite element method in the free form basins (in Russian). In V. M. Kaistrenko & A. B. Rabinovich (Eds.), *Theoretical and experimental studies of the long-wave processes* (pp. 104–114). Vladivostok: Far Eastern Scientific Center, Academy of Sciences of Soviet Union.

Medvedev, I. P., & Kulikov, E. A. (2016). Spectrum of mesoscale sea level oscillations in the northern Black Sea: Tides, seiches, and inertial oscillations. *Oceanology, 56*(1), 6–13. https://doi.org/10.1134/S0001437016010094.

Medvedev, I. P., Kulikov, E. A., & Rabinovich, A. B. (2017). Tidal oscillations in the Caspian Sea. *Oceanology, 57*(3), 360–375. https://doi.org/10.1134/S0001437017020138.

Medvedev, I. P., Rabinovich, A. B., & Kulikov, E. A. (2013). Tidal oscillations in the Baltic Sea. *Oceanology, 53*(5), 526–538. https://doi.org/10.1134/S0001437013050123.

Medvedev, I. P., Rabinovich, A. B., & Kulikov, E. A. (2016). Tides in three enclosed basins: The Baltic, Black and Caspian seas. *Frontiers in Marine Science*. https://doi.org/10.3389/fmars.2016.00046.

Mellor, G. L. (2004). *Users guide for a three-dimensional, primitive equation, numerical ocean model. Program in atmospheric and oceanic sciences*. Princeton: Princeton University.

Mungov, G. (1981). Study of the fluctuations of the sea level along the Bulgarian coast in medium-scale frequency range (in Bulgarian). *Khidrologiya i Meteorologiya, 2,* 20–21.

Munk, W. H., & Cartwright, D. E. (1966). Tidal spectroscopy and prediction. *Philosophical Transactions of the Royal Society A., 259*(1105), 533–581.

Orlov, A. Ya. (1923). About tides of the Black Sea in Odessa and Sevastopol (in Russian). *Zapiski po gidrografii, 47,* 141–161.

Parker, B. B. (2007). *Tidal analysis and prediction. NOAA spec. publ. NOS CO-OPS 3*. Maryland: Silver Spring.

Proudman, J. (1928). On the tides in a flat semicircular sea of uniform depth. *Monthly Notices of the Royal Astronomical Society, Geophysical Supplement, 2,* 32–43.

Pugh, D., & Woodworth, P. (2014). *Sea-level science: Understanding tides, surges, tsunamis and mean sea-level changes*. Cambridge: Cambridge University Press.

Rabinovich, A. B., & Medvedev, I. P. (2015). Radiational tides at the southeastern coast of the Baltic Sea. *Oceanology, 55*(3), 319–326. https://doi.org/10.1134/S0001437015030133.

Stammer, D., et al. (2014). Accuracy assessment of global barotropic ocean tide models. *Reviews of Geophysics, 52*(3), 243–282.

Sterneck, R. V. (1912). Über die Gezeiten des Schwarzen Meeres. *Anzeiger der Kaiserlichen Akademie der Wissenschaften. Wien (17 Oct.).*

Sterneck, R. V. (1922). Schematische Theorie der Gezeiten des Schwarzen Meeres. *Sitzungsberichte, Akademie der Wissenschaften in Wien, Matematisch-naturwissenschaftliche Klasse, 131,* 81–104.

Sterneck, R. V. (1926). Harmonische Analyse und Theorie der Gezeiten des Schwarzen Meeres. *Annalen der Hydrographie Maritimen Meteorologie, 54,* 289–296.

Thomson, R. E., & Emery, W. J. (2014). *Data analysis methods in physical oceanography* (3rd ed.). New York: Elsevier.

Yüce, H. (1993). Water level variations in the Sea of Marmara. *Oceanologica Acta, 16*(4), 335–340.

Yüce, H. (1996). On the variability of Mediterranean water flow into the Black Sea. *Continental Shelf Research, 16,* 1399–1413. https://doi.org/10.1016/0278-4343(95)00078-X.

Zalesny, V. B., Gusev, A. V., Lukyanova, A. N., & Fomin, V. V. (2016). Numerical modelling of sea currents and tidal waves. *Russian Journal of Numerical Analysis and Mathematical Modelling, 31*(2), 115–125.

(Received January 10, 2018, revised April 22, 2018, accepted April 24, 2018, Published online May 3, 2018)